



Surface Plasmon Resonance Enhancement of PbS Quantum Dot-Sensitized Solar Cells

Nikhil Chander¹

Received: 5 February 2019 / Accepted: 15 May 2019 / Published online: 20 May 2019
© Indian National Academy of Engineering 2019

Abstract

Lead sulfide (PbS)-sensitized quantum dot solar cells (QDSC) were fabricated using TiO₂ and TiO₂-Au plasmonic nanocomposite films by successive ionic layer adsorption and reaction (SILAR) method. The average size of gold nanoparticles (GNPs) used for fabricating nanocomposite films was ~ 15 nm. Thin plasmonic QDSC, with a film thickness of 10 μm, showed an increase of ~ 11% in photocurrent and ~ 6% in overall energy conversion efficiency compared to the device without GNPs. The improved performance of QDSCs is attributed to the increased absorption due to the plasmonic near-field effects of the incorporated GNPs. High-efficiency PbS/CdS-co-sensitized thick cells with 16 μm bilayer TiO₂ also showed improvement in photocurrent and efficiency. The results show that the plasmonic-enhanced absorption can be used to augment efficiency of QDSC devices in much the same fashion as that of dye-sensitized solar cells.

Keywords Gold nanoparticles · Plasmonics · Photovoltaics · Quantum dot-sensitized solar cells

Introduction

The sensitized solar cell technology is a versatile technique which offers the flexibility to use various kinds of sensitizers and provides an opportunity to make extremely thin devices. The recent progress in the field of perovskite solar cells (PSCs) has renewed the interest in quantum dot-sensitized solar cells (QDSCs) (Ye et al. 2015; Grätzel 2014). The origin of these types of solar cells can be traced back to the dye-sensitized solar cells (DSSCs). The successive ionic layer adsorption and reaction (SILAR) and chemical bath deposition (CBD) methods are simple and cost-effective ways of fabricating QDSCs. Many types of sensitized cells including CdS, CdSe, and PbS QDSCs have been fabricated using these techniques (Shengyuan et al. 2012; Duan et al. 2015). A combination of one or more of cadmium/lead chalcogenides is used for broadband solar spectrum absorption (Gonzalez-Pedro et al. 2013). In addition, a ZnS layer is applied using SILAR method to passivate the surface of

CdX/PbX quantum dots. This ZnS layer has been shown to improve performance of the QDSCs (Hachiya et al. 2012). QDSCs have the ability to provide large current values because of the low band-gap materials used in their fabrication which allow the harvesting of red/near infra-red (NIR) portion of the solar spectrum.

The use of metal nanoparticles (NPs) to improve the efficiency of dye-sensitized solar cells (DSSCs) has been studied by a number of research groups (Chander et al. 2014a, b; Dang et al. 2013; Brown et al. 2011). It has been observed that small metal NPs (diameter < 50 nm) and low concentrations (metal NP/TiO₂ weight ratio about 0.1–0.5 wt%) are best suited for absorption and consequently photocurrent enhancement of these devices. However, surprisingly, very few studies are available for plasmonic enhancement of photocurrent in QDSCs and PSCs (Jung and Kang 2011; Liu et al. 2011; Kawasaki and Tatsuma 2013; Pathak et al. 2017). Some papers have detailed the absorption enhancement process in quantum dot-metal NPs systems and suggested that photocurrent in QDSCs can be increased by scattering as well as the near-field enhancement due to plasmonic effects of metal NPs (Kawasaki and Tatsuma 2013; Lu et al. 2012; Beck et al. 2012; Batabyal et al. 2011). In the present study, we investigate the use of small gold nanoparticles (GNPs) of average size ~ 15 nm on the performance of PbS and PbS/CdS-co-sensitized QDSCs.

✉ Nikhil Chander
nikhil@iitbhillai.ac.in

¹ Department of Electrical Engineering and Computer Science, Indian Institute of Technology Bhilai, GEC Campus, Old Dhamtari Road, Sejbahar, Raipur, Chhattisgarh 492015, India

Experiment

Synthesis of Gold Nanoparticles

GNPs were synthesized by the well-known Turkevich method as described in a previous study (Chander et al. 2014a, b). Briefly, a 30 ml solution of 1 mM hydrogen tetrachloroaurate(III) trihydrate in de-ionized water was brought to boil on a hot plate. About 1% w/w trisodium citrate dihydrate aqueous solution was added to the boiling solution under stirring. Typically, for a 30 ml gold precursor solution in water, about 1.5 ml of 1% w/w trisodium citrate aqueous solution was added to obtain particle sizes of ~15 nm. About 1.5 ml of a 5% polyvinylpyrrolidone (PVP) aqueous solution was added to 30 ml of as-synthesized GNPs' solution and stirred overnight at room temperature. Following this step, the solution was centrifuged at 12,000 rpm for 20 min. Later, the supernatant was removed carefully and the GNPs collected at the bottom of centrifuge tubes were re-dispersed in ethanol. Nanoparticles dispersed in ethanol were mixed with TiO₂ paste for making plasmonic paste consisting of Au-TiO₂ in a particular weight ratio. In the present work, an Au-TiO₂ weight ratio of ~0.5 wt% has been used.

Fabrication of TiO₂ and TiO₂-Au Photoanodes

The TiO₂ photoanodes were prepared using a previously reported procedure (Chander and Komarala 2017). The experimental methods are presented here in brief. Fluorine-doped tin-oxide (FTO)-coated glass slides were cleaned using soap water, de-ionized water and propan-2-ol in an ultrasonic bath and dried in the air. A thin (~80 nm) compact layer of TiO₂ was deposited on FTO substrates at 450 °C by spray pyrolysis of titanium diisopropoxide bis(acetylacetonate) (Sigma-Aldrich) diluted in ethanol. Transparent titania paste (Dyesol, 18-NR-T) was deposited on compact TiO₂-coated FTO substrates by the doctor blade method. The geometric area of the films thus fabricated was 1.21 cm². Gold nanoparticles of size ~15 nm mixed with titania paste in an Au/TiO₂ weight ratio of ~0.5 wt% were used for making TiO₂-Au films. The thickness of the mesoporous layer thus prepared was adjusted to ~10 or ~12 μm by repeating the doctor blade process. The films were sintered at 500 °C in the air for 30 min. A scattering layer of ~4 μm was coated on top of the mesoporous layer using the doctor blade method and the films were sintered again at 500 °C. Following this step, the films were immersed in a 40 mM aqueous TiCl₄ solution at 70 °C for 30 min. After this, the films were annealed at 500 °C in the air. The films were ready

for sensitization after this step. For optical studies, TiO₂ films with a thickness of ~6 μm and no scattering layer were used.

Preparation and Assembly of QDSCs

The procedure outlined by Hachiya et al. was used for sensitizing TiO₂ and TiO₂-Au films with PbS/ZnS (Hachiya et al. 2012). The films used for PbS/ZnS QDSCs had a thickness of ~10 μm. The films were immersed in a 0.05 M aqueous lead acetate solution for 25 s and then rinsed with de-ionized (DI) water. Next, the films were immersed in a 0.05 M aqueous Na₂S solution for 25 s and rinsed with DI water. This coating cycle was then repeated. After adsorption of the PbS QDs, the electrodes were passivated by ZnS using the SILAR method in a zinc acetate solution (0.1 M in water) for 1 min and an Na₂S solution (0.1 M in water). Ten cycles of the ZnS SILAR coating were performed.

A previously reported procedure was followed for deposition of PbS/CdS/ZnS on the TiO₂ films (Gonzalez-Pedro et al. 2013). In brief, 0.02 M of lead acetate, 0.05 M of cadmium acetate, and 0.1 M of zinc acetate in methanol were used for metal precursors. Correspondingly, the same concentrations of sodium sulfide in 1:1 methanol-water were used as the sulfur source. Two cycles of SILAR were employed for PbS deposition, five cycles for CdS deposition and two cycles for ZnS deposition. Each cycle consisted of two steps of 1 min each in which the titania films were first dipped in metal precursor solution and then dipped in the sulfide solution.

The CuS counter electrode was prepared by spin coating a drop (~0.5 ml) of 0.5 M Cu(NO₃)₂ methanol solution on FTO substrates followed by coating 1 M Na₂S solution in 1:1 water-methanol. The procedure was repeated three times and the counter electrode was rinsed with de-ionized water and dried using an air gun. The electrolyte consisted of 1 M Na₂S, 1 M S, and 0.1 M NaOH in DI water. The photoelectrode and the counter electrode were pressed together in a sandwich configuration and electrolyte was injected using a pipette. Scotch tape was used as a spacer layer and the two electrodes were clamped using binder clips.

Instruments

UV-visible spectra were recorded using Perkin Elmer Lambda 1050 spectrophotometer. Philips system was used for X-ray diffraction (XRD) measurements. Transmission electron micrograph (TEM) images were captured by Tecnai G2 20 electron microscope. The current density versus voltage curves were recorded using a 450 W Oriel Class AAA solar simulator and Keithley 2440 source meter. A calibrated silicon solar cell was used for reference. The active area of the solar cells was 1 cm² and was defined using a

black-coloured mask. All the measurements were performed at room temperature in the air.

Results and Discussion

The extinction spectrum of the synthesized GNPs dispersed in water is shown in Fig. 1. The transmission electron micrograph (TEM) in the inset shows that the size of the particles is ~ 15 nm. The particles are monodispersed and show no agglomeration. The peak in the spectrum corresponds to the surface plasmon resonance (SPR) of GNPs in water medium and occurs at 520 nm. More discussion on GNPs is presented later in the manuscript.

The XRD spectra of bare TiO₂ film on FTO glass, PbS-sensitized TiO₂ film, and PbS/ZnS-sensitized TiO₂ film are shown in Fig. 2. The peaks corresponding to FTO and TiO₂ are marked clearly to distinguish them from peaks of PbS and ZnS. The broad peaks at 30° and 43° correspond to the (200) and (220) reflection planes of the PbS galena crystal. This confirms the formation of PbS QDs on the TiO₂ electrode. After ten cycles of ZnS coating, an increase in intensity around 29° is observed which corresponds to the (111) reflection plane of the ZnS sphalerite crystal. It implies that the PbS QDs are covered with ZnS after ten SILAR cycles. The XRD data show that SILAR is an efficient technique for coating chalcogenide films on mesoporous TiO₂ layer.

The photovoltaic (PV) parameters of the PbS/ZnS solar cells are shown in Table 1. These data are for eight devices: four control and four plasmonic solar cells. The enhancements in photocurrent and efficiency are outside the error

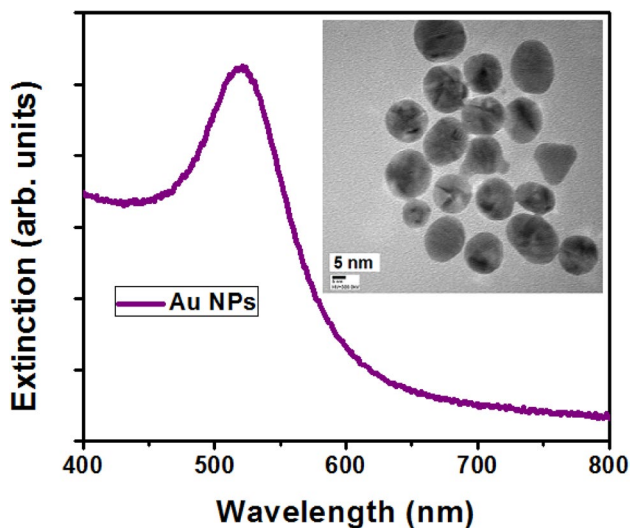


Fig. 1 Extinction spectrum of gold nanoparticles of size ~ 15 nm dispersed in water. The peak corresponding to surface plasmon resonance of gold nanoparticles occurs at 520 nm. Inset shows the transmission electron micrograph of the synthesized nanoparticles

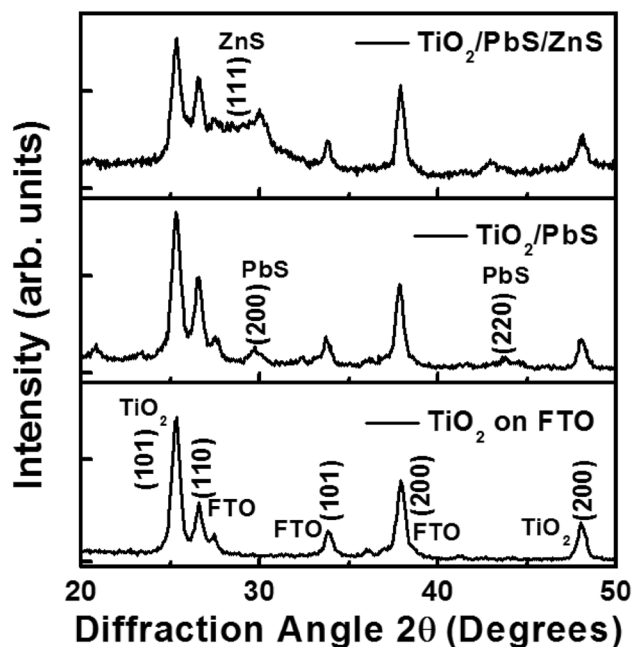


Fig. 2 X-ray diffraction spectra of PbS/ZnS film coated on TiO₂/FTO glass

margins. The current density (*J*) versus voltage (*V*) curves of the devices with the highest efficiency in PbS/ZnS case are shown in Fig. 3. The best control device has *J*_{SC} of 11.6 mA/cm² compared to the 12.9 mA/cm² of the best plasmonic device. The percent enhancement in photocurrent is ~ 11% for the plasmonic device. The efficiencies are low, because the active layer has PbS as the only sensitizer. In addition, the active layer thickness of these devices is about 10 μm, which is less than the optimum thickness required for obtaining high efficiency. However, the effect of GNPs is evident for the plasmonic QDSCs, which show a higher photocurrent. This increase is due to the improved light absorption in the device brought about by the near-field enhancement effects of the GNPs. The transmittance values as a function of wavelength for TiO₂, TiO₂-Au, TiO₂/PbS/ZnS, and TiO₂-Au/PbS/ZnS films are shown in Fig. 4. It is clear from this figure that the films containing GNPs have lower transmittance. A low transmittance indicates that the film has a higher absorption. The increased absorption due to plasmonic effects is responsible for the increased photocurrent observed for the case of plasmonic QDSCs.

The *J*-*V* curves of the PbS/CdS/ZnS QDSCs with and without the GNPs are shown in Fig. 5a. The dark *J*-*V* curves are also shown in Fig. 5b. The dark curves are almost overlapping and there is no noticeable difference. The devices with highest efficiencies in each case are shown. Table 1 shows the photovoltaic parameters of four control devices and four plasmonic devices (total eight devices). In this case, the photocurrent and efficiency

Table 1 Photovoltaic parameters of quantum dot-sensitized solar cells fabricated in the present work

Type of device ^a	Short-circuit current density (mA/cm ²)	Open-circuit voltage (mV)	Fill factor (%)	Efficiency (%)
PbS/ZnS				
Control PbS/ZnS (four devices)	11.43 ± 0.12	325 ± 0.82	33.75 ± 0.50	1.25 ± 0.03
Plasmonic PbS/ZnS (four devices)	12.78 ± 0.08	327.25 ± 2.22	32.25 ± 0.50	1.35 ± 0.02
PbS/CdS/ZnS				
Control PbS/CdS/ZnS (four devices)	21.67 ± 0.10	395 ± 5.77	42.72 ± 0.61	3.66 ± 0.03
Plasmonic PbS/CdS/ZnS (four devices)	21.78 ± 0.13	404.5 ± 5.26	43.18 ± 0.24	3.80 ± 0.06

The average values of four devices (of each type, total 16 devices) along with standard deviations are shown. The active areas of all the devices are 1 cm²

^aControl device has no gold nanoparticles. Plasmonic device has gold nanoparticles in Au/TiO₂ weight ratio of ~0.5 wt%

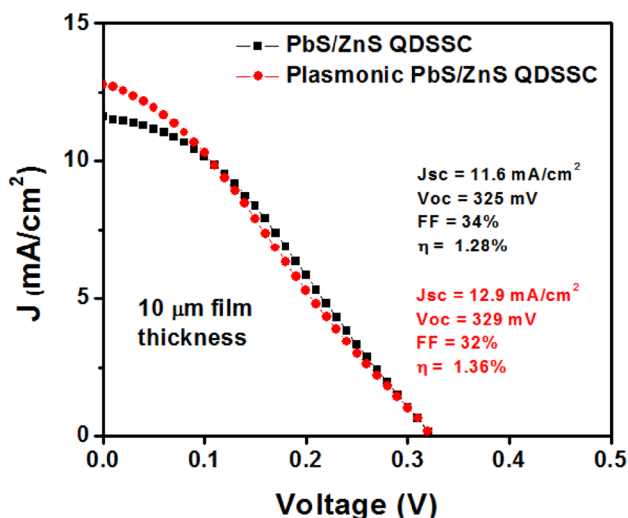


Fig. 3 Current density (J) versus voltage (V) curves of normal and plasmonic PbS/ZnS quantum dot-sensitized solar cells

values are higher than the previous case (with only PbS), because now two sensitizers, or light harvesting materials, are present—PbS and CdS. In addition, the TiO₂ film thickness is 12 µm plus 4 µm of scattering layer (composed of large-sized TiO₂ nanoparticles), making an optically thick layer. However, in the present case, the plasmonic device does not exhibit a significantly higher photocurrent than the control device. In fact, Table 1 shows that although the photocurrent enhancement is provided by GNPs, it is not outside the error margins. This implies that both the size and the concentration of GNPs may need to be optimized to get better results. However, still, the photocurrent value close to 22 mA/cm² is comparable with the highest efficiency perovskite solar cell fabricated to date, which had a J_{SC} of about 24 mA/cm² (Yang et al. 2015). An enhancement in photocurrent, although small, has been observed at such high values, which shows that plasmonics may turn out to be a promising technique to

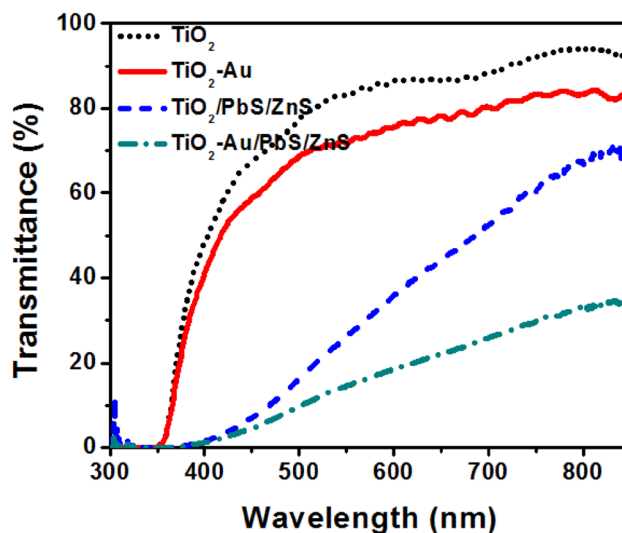


Fig. 4 Transmittance as a function of wavelength for four different types of films. The decreased transmittance, indicating an increase in absorption, is evident for films containing Au nanoparticles

further enhance the efficiency of QDSCs as well as the fast emerging perovskite solar cells.

The size and concentration of GNPs need to be optimized to get the best performance from plasmonic QDSCs. According to Mie theory, under quasi-static approximation, the absorption and scattering cross sections of a spherical metal nanoparticle can be expressed as (Bohren and Huffman 1998)

$$C_{\text{abs}} = k \operatorname{Im}(\alpha) \quad (1)$$

$$C_{\text{scat}} = \frac{k^4}{6\pi} |\alpha|^2, \quad (2)$$

where α is the polarizability of the metal nanoparticle given by

$$\alpha = 4\pi r^3 [(\epsilon_p - \epsilon_m) / (\epsilon_p + 2\epsilon_m)]. \quad (3)$$

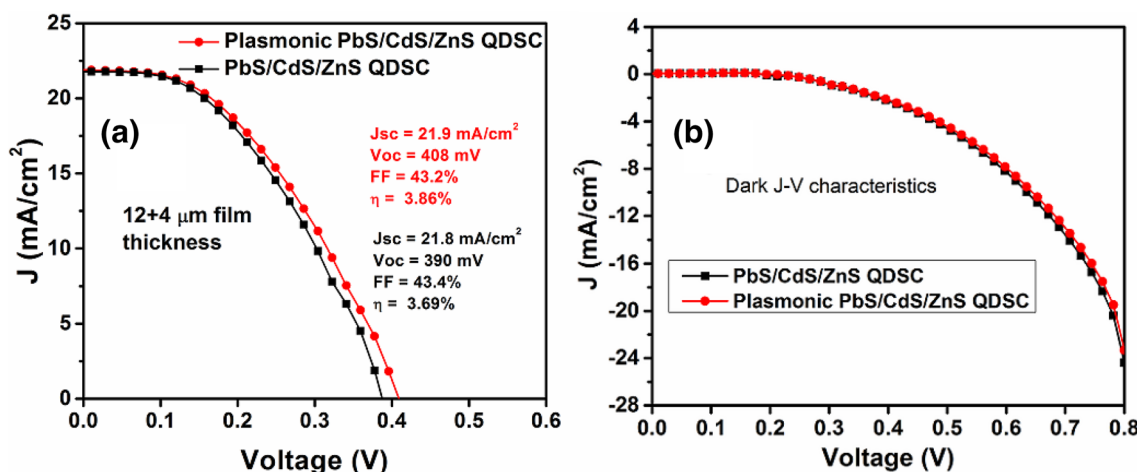


Fig. 5 Current density (J) versus voltage (V) curves of normal and plasmonic PbS/CdS/ZnS quantum dot-sensitized solar cells in **a** light (AM1.5G illumination) and **b** dark conditions

In Eq. (3), r is the radius of the metal nanoparticle, ϵ_p is the dielectric constant of the particle, and ϵ_m is the dielectric constant of the surrounding medium. It can be seen from the above equations that the scattering is proportional to the square of the polarizability, which in turn is proportional to the cube of the particle size (radius). From this analysis, it is easy to see that the scattering is proportional to sixth power of the radius of the particle. Due to this reason, for larger particles, scattering dominates over absorption and is the prominent extinction mechanism. Extinction cross section, C_{ext} , is defined as a summation of absorption and scattering cross sections:

$$C_{ext} = C_{abs} + C_{scat} \tag{4}$$

Efficiency factors or efficiencies for extinction, absorption and scattering may be defined as (Bohren and Huffman 1998):

$$Q_{ext} = C_{ext}/G, \quad Q_{abs} = C_{abs}/G, \quad Q_{scat} = C_{scat}/G, \tag{5}$$

where G is the cross-sectional area of the metal particle projected on a plane perpendicular to the incident electromagnetic beam. In the present case of a spherical metal nanoparticle with radius r , the factor G is given by, $G = \pi r^2$.

The absorption, scattering, and extinction efficiencies of GNPs of varying sizes (5 nm, 15 nm, 50 nm, and 100 nm) are shown in Fig. 6. The calculations have been performed using a software tool freely available from reference (<http://www.philiplaven.com/mieplot.htm>). The simulations have been performed by taking the refractive index values at four different wavelengths from the data of Sanchez et al. for simplicity of calculations (Sanchez et al. 2013). The values of refractive index are: 1.72 at 435 nm, 1.68 at 480 nm, 1.64 at 587 nm, and 1.62 at 706 nm. These values are less than the refractive index of anatase TiO₂ (~2.48) and approximate

the medium around the gold nanoparticles which consists of anatase TiO₂ and air.

The simulations clearly show that scattering is dominant for large GNPs of size 100 nm and absorption dominates for smaller particle sizes. In fact, we do not observe any scattering for the case of 5 and 15 nm GNPs. It indicates that only absorption contributes towards extinction of incident light for these small-sized particles embedded in TiO₂. Mid-sized GNPs (50 nm) show the highest absorption efficiency (see Fig. 6a). These results are a direct consequence of the size dependence of scattering and absorption, as given by Eqs. (1)–(3). For sensitized type of solar cells, as presented in this work, the increased absorption is more beneficial than scattering (Chander et al. 2014a, b). In GNPs, the conduction band electrons oscillate due to the electric field of the incident electromagnetic radiation and give rise to an oscillating electric field (the so-called near field) localized around the nanoparticles. This near field can excite the sensitizers (PbS/CdS in the present case) more strongly than the incident far-field light and provides photocurrent enhancement. This near field depends on a number of parameters, size being one of the major ones. Therefore, intermediate-sized GNPs (of the order of 50 nm) are best suited for plasmonic DSSC/QDSC applications. Further research work is ongoing in this direction.

Conclusion

Gold nanoparticles of size ~15 nm have been used in the present work to demonstrate the plasmonic enhancement of photocurrent for PbS and PbS/CdS quantum dot-sensitized solar cells. The enhancements in photocurrent and efficiency have been observed for multiple devices and show consistent

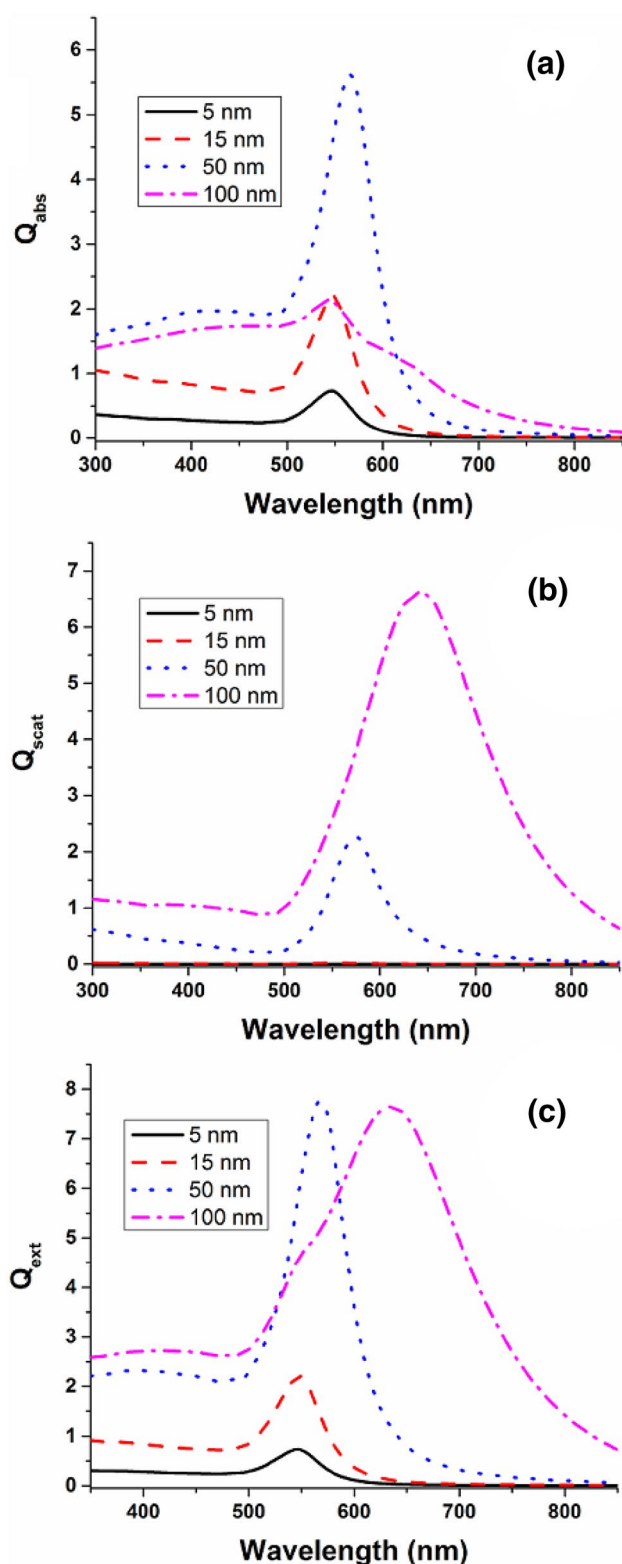


Fig. 6 **a** Absorption, **b** scattering, and **c** extinction efficiency curves for spherical gold nanoparticles of various sizes embedded in TiO_2 -Au medium. The Mie theory calculations have been performed using a free software tool taken from <http://www.philiplaven.com/mieplot.htm>). The values of refractive index have been taken from Sanchez et al. (2013)

trend. Further optimization of size and concentration of the GNPs would lead to still higher efficiencies in quantum dot-sensitized solar cells. The general approach mentioned in the paper can also be used to realize high-efficiency plasmonic perovskite solar cells.

Acknowledgements N. Chander thanks Dr. Vamsi Krishna Komarala, Associate Professor, Centre for Energy Studies, IIT Delhi, India, for I-V characterization of solar cells. The research was supported in part by the Department of Science and Technology, Govt. of India, under Inspire Faculty Award Number DST/INSPIRE/04/2015/003204.

Funding This work was supported in part by the Department of Science and Technology, Govt. of India, under Inspire Faculty Award Number DST/INSPIRE/04/2015/003204.

References

- Batabyal S, Makhal A, Das K, Raychaudhuri AK, Pal SK (2011) Ultrafast dynamics of excitons in semiconductor quantum dots on a plasmonically active nano-structured silver film. *Nanotechnology* 22:195704
- Beck FJ, Garcia de Arquer FP, Bernechea M, Konstantatos G (2012) Electrical effects of metal nanoparticles embedded in ultra-thin colloidal quantum dot films. *Appl Phys Lett* 101:041103
- Bohren CF, Huffman DR (1998) *Absorption and Scattering of Light by Small Particles*. Wiley, New York, pp 136–141
- Brown MD, Suteewong T, Santosh RS, D’Innocenzo V, Petrozza A, Lee M, Wiesner U, Snaith HJ (2011) Plasmonic dye-sensitized solar cells using core-shell metal-insulator nanoparticles. *Nano Lett* 11:438–445
- Chander N, Komarala VK (2017) Fabrication and characterization of dye sensitized solar cells: a photographic guide. *Indian J Pure Appl Phys* 55:737–744
- Chander N, Singh P, Khan AF, Dutta V, Komarala VK (2014a) Photocurrent enhancement by surface plasmon resonance of gold nanoparticles in spray deposited large area dye sensitized solar cells. *Thin Solid Films* 568:74–80
- Chander N, Khan AF, Thouti E, Sardana SK, Chandrasekhar PS, Dutta V, Komarala VK (2014b) Size and concentration effects of gold nanoparticles on optical and electrical properties of plasmonic dye sensitized solar cells. *Sol Energy* 109:11–23
- Dang X, Qi J, Klug MT, Chen PY, Yun DS, Fang NX, Hammond PT, Belcher AM (2013) Tunable localized surface plasmon-enabled broadband light-harvesting enhancement for high-efficiency panchromatic dye-sensitized solar cells. *Nano Lett* 13:637–642
- Duan J, Zhang H, Tang Q, He B, Yu L (2015) Recent advances in critical materials for quantum dot-sensitized solar cells: a review. *J Mater Chem A* 3:17497–17510
- Gonzalez-Pedro V, Sima C, Marzari G, Boix PP, Gimenez S, Shen Q, Dittrich T, Mora-Sero I (2013) High performance PbS Quantum Dot Sensitized Solar Cells exceeding 4% efficiency: the role of metal precursors in the electron injection and charge separation. *Phys Chem Chem Phys* 15:13835–13843
- Grätzel M (2014) The light and shade of perovskite solar cells. *Nat Mater* 13:838–842
- Hachiya S, Shen Q, Toyoda T (2012) Effect of ZnS coatings on the enhancement of the photovoltaic properties of PbS quantum dot-sensitized solar cells. *J Appl Phys* 111:104315
- Jung MH, Kang MG (2011) Enhanced photo-conversion efficiency of CdSe-ZnS core-shell quantum dots with Au nanoparticles on TiO_2 electrodes. *J Mater Chem* 21:2694–2700

- Kawasaki T, Tatsuma T (2013) Enhancement of PbS quantum dot-sensitized photocurrents using plasmonic gold nanoparticles. *Phys Chem Chem Phys* 15:20247–20251
- Liu L, Wang G, Li Y, Li Y, Zhang JZ (2011) CdSe quantum dot-sensitized Au/TiO₂ hybrid mesoporous films and their enhanced photoelectrochemical performance. *Nano Res.* 4:249–258
- Lu HF, Mokkapat S, Fu L, Jolley G, Tan HH, Jagadish C (2012) Plasmonic quantum dot solar cells for enhanced infrared response. *Appl Phys Lett* 100:103505
- Pathak NK, Chander N, Komarala VK, Sharma RP (2017) Plasmonic perovskite solar cells utilizing Au@ SiO₂ core-shell nanoparticles. *Plasmonics* 12:237–244
- Sanchez VM, Martínez ED, Martínez Ricci ML, Troiani H, Soler-Illia GJAA (2013) Optical properties of Au nanoparticles included in mesoporous TiO₂ thin films: a dual experimental and modeling study. *J Phys Chem C* 117:7246–7259
- Shengyuan Y, Nair AS, Peining Z, Ramakrishna S (2012) Electrospun TiO₂ nanostructures sensitized by CdS in conjunction with CoS counter electrodes: Quantum dot-sensitized solar cells all prepared by successive ionic layer adsorption and reaction. *Mater Lett* 76:43–46
- www.philiplaven.com/mieplot.htm. Accessed 5 June 2018
- Yang WS, Noh JH, Jeon NJ, Kim YC, Ryu S, Seo J, Seok SI (2015) High-performance photovoltaic perovskite layers fabricated through intramolecular exchange. *Science* 348:1234–1237
- Ye M, Wen X, Wang M, Iocozzia J, Zhang N, Lin C, Lin Z (2015) Recent advances in dye-sensitized solar cells: from photoanodes, sensitizers and electrolytes to counter electrodes. *Mater Today* 18:155–162

Publisher's Note Springer Nature remains neutral with regard to jurisdictional claims in published maps and institutional affiliations.